8-2023

Towards Deposition of Iron & Nickel Onto Cadmium Selenide/ Cadmium Sulfide Nanorods

Rajib Nath

TOWARDS DEPOSITION OF IRON AND NICKEL ONTO CADMIUM SELENIDE/CADMIUM SULFIDE NANORODS

A thesis submitted in partial fulfillment
of the requirements for the degree
Master of Science

Department of Chemistry
Western Kentucky University
Bowling Green, Kentucky

By
Rajib Nath

August 2023

TOWARDS DEPOSTION OF IRON AND NICKEL ONTO CADMIUM SULFIDE/CADMIUM SELENIDE NANORODS

Rajib Nath

Date Recommended 7/6/2023

DocuSigned by:
Dr. Lawrence Hill
A9DCB9E86152404...
Chair

DocuSigned by:
Dr. Bangbo Yan
4D62F99FCFF840C...
Committee Member

DocuSigned by:
Dr. Matthew Mc
060FA5FC6F1241C...
Committee Member

Committee Member

DocuSigned by:
Dr. Ranjit Koodali
8F8057903E39448...
Associate Provost for Research and Graduate Education

ABSTRACT

TOWARDS DEPOSITION OF IRON AND NICKEL ONTO CADMIUM SELENIDE/CADMIUM SULFIDE NANORODS

Metal-semiconductor hybrids have been studied extensively as photocatalysts for the water-splitting reaction to generate hydrogen gas and oxygen gas to use as a renewable energy source. The semiconductor component converts light into electrochemical energy, while the metal component provides a site for chemical reactions with water. Here, the choice of metal can have a significant impact on the efficiency of the catalyst. Platinum efficiently catalyzes the water-splitting reaction and is therefore commonly used in metal-semiconductor hybrids to generate hydrogen. Platinum is very expensive, which motivates research into improving less costly metals like iron or nickel that do not have nearly the catalytic performance of platinum. Recent results have shown that iron and nickel can be combined into structures with oxygen that behave similarly to platinum as catalysts for water-splitting on electrodes, but these materials have not been tested as replacements for platinum in metal-semiconductor photocatalysts. This thesis will describe our work toward synthesizing metal-semiconductor hybrids using iron and nickel to replace platinum.

Keywords: [water splitting, photocatalyst, electrode, semiconductor]

ACKNOWLEDGMENTS

I would like to express my sincere gratitude to my research advisor, Dr. Lawrence Hill, for his invaluable guidance, support, effort, and instruction. I also extend my thanks to Dr. Mathew Nee and Dr. Bangbo Yan for their valuable feedback, as well as Dr. Jhon Andersland, Dr. Dali Qian, and Jillian Cramer for their support. I am also thankful to all the members of the research group. Lastly, I would like to express my appreciation to the faculty members and staff of the Chemistry department at Western University.

TABLE OF CONTENTS

LIST OF TABLES

LIST OF FIGURES

Chapter 1. Introduction and overview of water splitting

Fossil fuels like coal, oil, and gas are exhaustible and produce different kinds of greenhouse gases such as carbon dioxide.[1] Hydropower, solar energy, wind energy, and bioenergy are common sources of renewable energy derived from inexhaustible natural sources.[2,3] One approach is to harvest solar energy by photocatalysis to obtain hydrogen gas from water, where hydrogen is a renewable fuel that produces no carbon dioxide when consumed. These photocatalysts frequently use platinum to facilitate hydrogen production, and in our research, we are trying to develop a new photocatalyst where we replace platinum with more abundant metals like iron and nickel. This chapter will introduce the concept of water splitting to produce hydrogen gas as well as design features of photocatalysts relevant to this project.

Water splitting is a chemical reaction where the water breaks down into oxygen and hydrogen, the latter of which can be a source of renewable energy.[4]

$$2H_2O \longrightarrow 2H_2 + O_2$$

$$\text{OER half reaction: } 4OH^- \longrightarrow 4e^- + 2H_2O + O_2$$

$$\text{HER half reaction: } 2H_2O + 4e^- \longrightarrow 4OH^- + 2H_2$$

The water splitting reaction is a combination of two half reactions. One half reaction is the hydrogen evolution reaction (HER) and the other half reaction is the oxygen evolution reaction (OER). Water is reduced to hydrogen in the hydrogen evolution reaction (HER) and oxidized to oxygen in the oxygen evolution reaction (OER).

The water splitting reaction requires a standard Gibbs free energy of 237 kJ/mol.[5] This is the minimum energy theoretically required to get hydrogen from the water splitting reaction, while the rate of water splitting is controlled by the kinetic barrier determined by the reaction

conditions. Catalysts are used to lower the activation energy required for water splitting (Figure 1.1). Hydrogen can be produced from water by electrochemical or photocatalytic means, as described in the following sections.

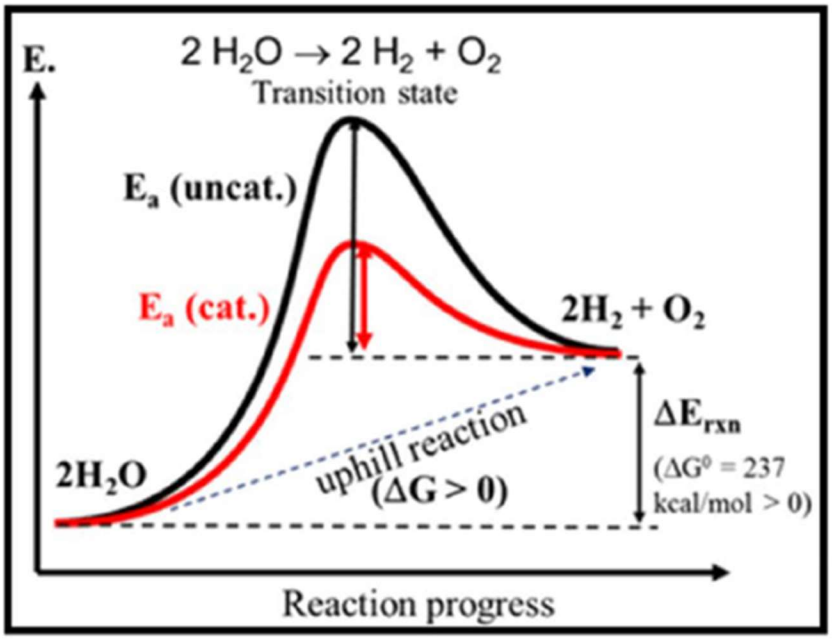

Figure 1.1 A reaction coordinate diagram for water splitting reaction. The water splitting reaction is an uphill reaction. It shows the presence of a catalyst (red line) in the reaction lower the activation energy compared to a reaction without a catalyst (black line). This figure is reproduced from reference 4.

1.1 Electrochemical water splitting

Electrochemical water splitting is one of the approaches to produce hydrogen and oxygen. Electrochemical water splitting is conducted using an electrochemical cell which consists of two electrodes (anode and cathode) that relate to the electrical power source (Figure 1.2). An oxidation reaction takes place at the anode generating oxygen gas and electrons, and then a reduction reaction takes place between hydrogen cations and electrons from the cathode to form hydrogen gas. Here, the electrodes can incorporate catalysts to lower the voltage required to achieve water splitting.

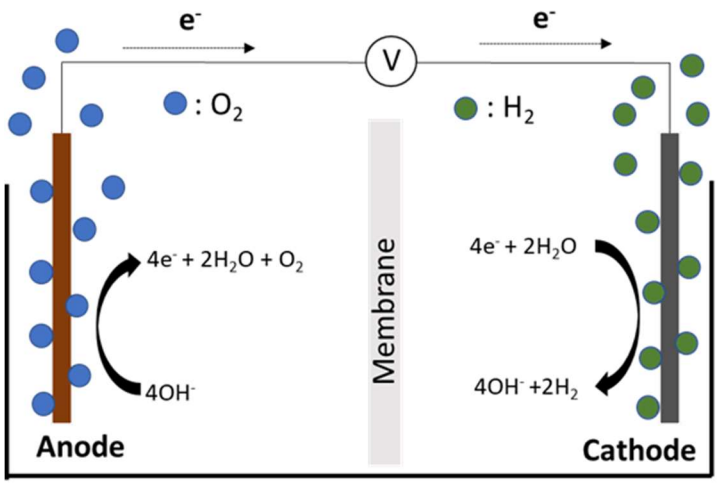

Figure 1.2 A schematic diagram of electrochemical water splitting in an alkaline solution. An electrochemical cell consists of two electrodes (anode and cathode) connected to an external power supply. Oxidation reaction takes place at the anode and produces oxygen while reduction reaction happens at the cathode and generates hydrogen.

The hydrogen evolution reaction (HER) commonly uses platinum-based electrodes due to the lowest overpotential of platinum among all metals, while Ir/Ru-based compounds are utilized for oxygen evolution reaction (OER).[6] Other noble metals like Pd, Ru, and Rh can also act as catalysts in hydrogen evolution reactions (HER), but they are not cost-effective and are less abundant on Earth.[4] To replace these noble metals, researchers have developed electrocatalysts based on metal oxides, non-noble metal alloys, metal sulfides, carbides, and phosphides for HER.[6 7] $Ni(OH)_2$ decorated platinum surface shows enhanced hydrogen production compared to bare platinum.[8]

Recently, it was reported that Ni-Fe nanoparticles with nickel-iron oxide interface demonstrated catalytic performance comparable with platinum on carbon catalyst for electrochemical water splitting reaction.[9] Figure 1.3 shows the formation of Ni-Fe nanoparticles through oleate-assisted micelle formation and a schematic presentation of Ni and Fe nanoparticles. The enhancement of hydrogen production is caused by the coupling effect between the iron oxide and nickel at the

interface.[9] The surface area to volume ratio for nanoparticles influences the properties of the material. The surface area to volume ratio increases when the size of particles is decreased. It means that for a certain volume when the particles are smaller specific surface area increased compared to bulk materials due to this Ni-Fe nanoparticle with nickel and iron oxide interface facilitating the electrochemical water splitting reaction.

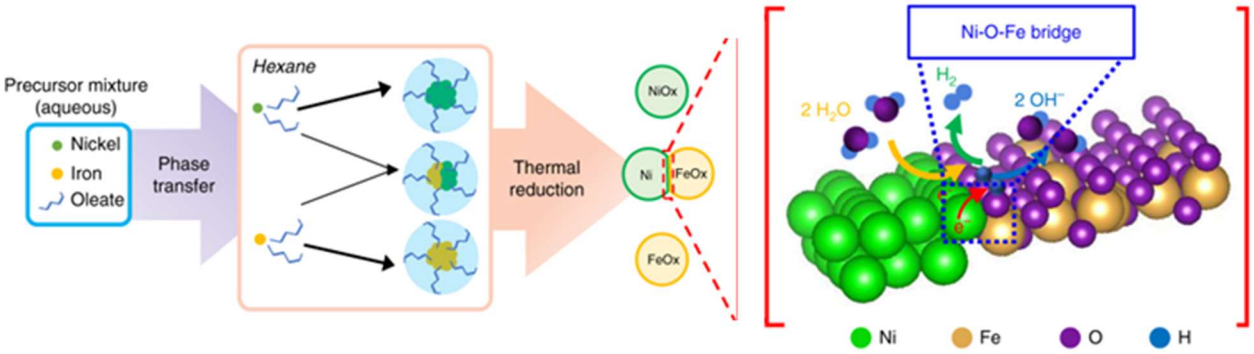

Figure 1.3 Formation of Ni-Fe nanoparticles through oleate-assisted micelle formation and schematic presentation of Ni and Fe nanoparticles. This figure was reproduced from reference 9.

1.2 Photocatalytic water splitting

A photoelectrochemical water splitting by using an electrochemical cell with Pt/TiO_2 electrode was reported by Akira Fujishima and Keinchi Honda in 1972 (Figure 1.4).[10,11] When the surface of TiO_2 was irradiated with light, current flow was recorded. The direction of current flow was platinum electrode to TiO_2 electrode through the external circuit where OER occurs at the TiO_2 electrode while HER occurs at the platinum electrode.[11]

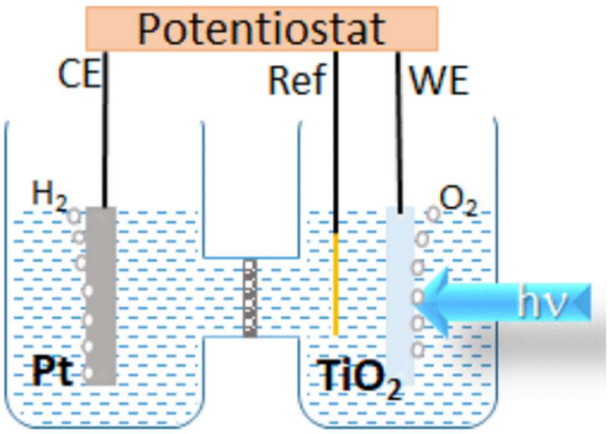

Figure 1.4 A schematic electrochemical cell for photoelectrochemical water splitting using a TiO_2 semiconductor photoanode working electrode (WE) with a platinum counter electrode (CE), and reference electrode. This figure is reproduced from reference 10.

Photocatalytic water splitting is favorable when the photocatalyst has a more negative conduction band edge than the redox potential of H^+/H_2 (0 V vs. NHE, pH=0) and a more positive valence band edge than the redox potential of O_2/H_2O (1.23 V vs. NHE, pH=0).[12]

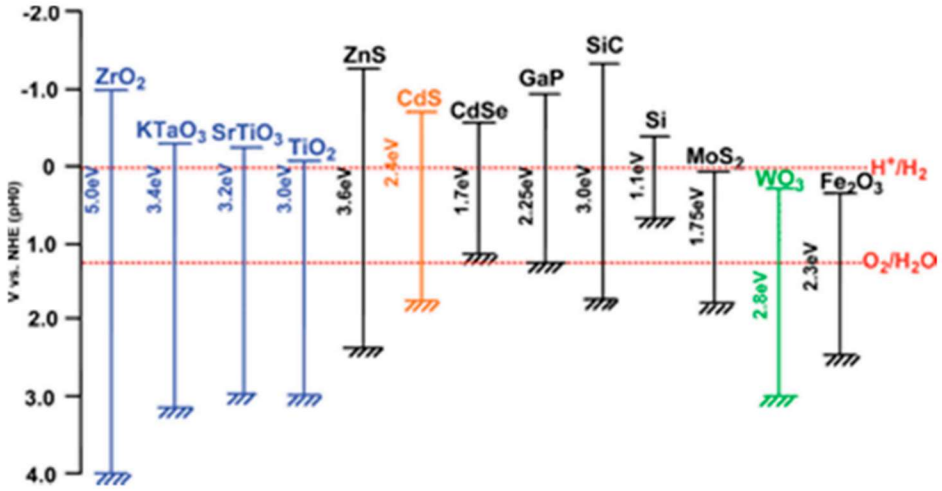

Figure 1.5 Bandgap, valence band, and conduction band of different semiconductors on a potential scale (v) versus the normal hydrogen electrode (NHE). This figure is reproduced from reference 13.

Photocatalytic hydrogen production depends on light harvesting. Figure 1.5 shows the band gaps of different semiconductors with redox potentials.[13] Wide bandgap semiconductors like TiO_2 harvest light from the ultraviolet region to get photocatalytic hydrogen. This small portion of light harvesting compared to the full range solar spectrum is one of the limitations of these wide bandgap semiconductors. Elemental doping, surface sensitization, and heterojunction structure construction are different approaches to utilizing the visible range light for photocatalytic hydrogen production.[14]

The activity of a photocatalyst also depends on the separation of photogenerated charges. In photocatalytic water splitting, a semiconductor absorbs light to generate electron-hole pairs. Then charge separation and migration to the surface of the photocatalyst occurs and electrons and holes react with water and produce hydrogen and oxygen. Electron/hole recombination in photocatalytic water splitting reaction can limit the photocatalytic activity of a photocatalyst.

The photocatalytic activity of a photocatalyst is limited by electron hole recombination. The transfer of photogenerated charges to the surface of a photocatalyst or their recombination is influenced by crystal size, surface properties, and structural defects. By altering the size, composition, and shape of nanoscale semiconductor materials, their properties can be changed from those of bulk materials.[15] Nanomaterials of suitable band gap energy can be achieved by changing their size and changing their solar light harvesting performance relative to bulk materials.[15] The surface area of semiconductor photocatalysts made from nanomaterials is another important feature. The number of surface atoms per unit mass increases when the size of the material is decreased. Additionally, photocatalytic activity is enhanced by surface

roughness, which increases the specific surface area and provides more active sites for photocatalytic reactions.[16]

1.2.1 Metal-semiconductor heterojunctions

Metal-metal alloys, metal oxides, metal sulfides, and metal nitrides are attached to semiconductors to get metal-semiconductor heterojunction materials that enhance light absorption, limit electron-hole recombination rate, and change electronic properties. A cartoon representation of these metal-semiconductor heterojunctions is shown in Figure 1.6-A.[17] In these materials, electrons promoted to the conduction band of the semiconductor can migrate to the metal-semiconductor interface where the electron can transfer from the higher energy conduction band of the semiconductor to the available lower energy states of the metal. Recombination of the electron and hole within the semiconductor is also possible, and the efficiency of these catalysts is influenced by the relative rates of recombination versus electron transfer to the metal cocatalyst.

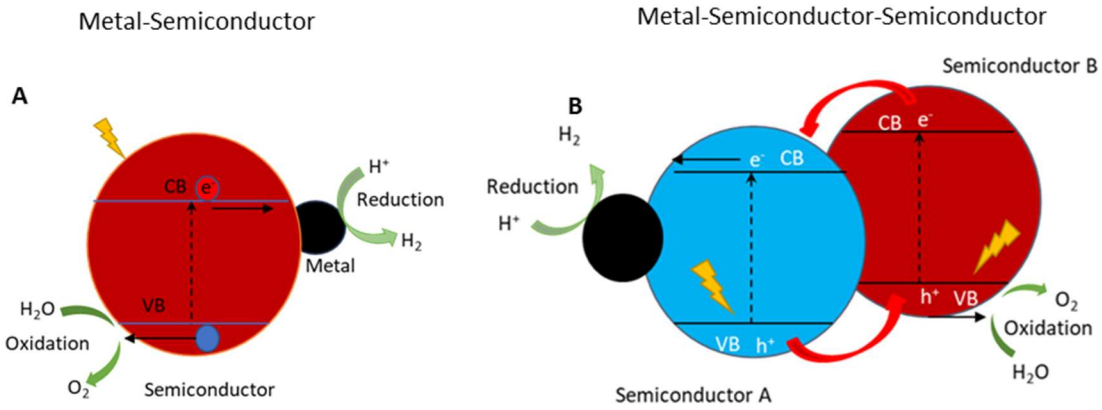

Figure 1.6. A schematic representation of A) metal-semiconductor heterojunction, and B) metal-semiconductor-semiconductor heterojunction.

Materials with both semiconductor-semiconductor heterojunctions and metal-semiconductor heterojunctions have also been investigated as photocatalysts that benefit from additional charge separation by driving the holes to the semiconductor having the higher energy valence band edge, while the electrons migrate to the other semiconductor followed by the metal cocatalyst (Figure 1.6-B). This additional spatial separation of charges helps to limit electron/hole recombination which can increase light harvesting efficiency.[21]

Platinum is one of the most common metals used for metal-semiconductor heterojunction materials due to platinum helps to trap electrons from the semiconductor's conduction band which limits electron-hole recombination and enhances the light harvesting efficiency.[18] It was reported that platinum decorated titanium dioxide acts as a photocatalyst, and TiO_2 nanoparticles decorated with platinum produced roughly double the amount of hydrogen from water compared to bare titanium dioxide under the same illumination conditions.[18] This performance from platinum decorated titanium dioxide is due to electrons being transferred from titanium oxide to platinum where hydrogen cations are reduced to hydrogen gas. Platinum enhances photocatalytic activity compared to bare semiconductors, but limited availability and high cost limit the application of materials that use platinum. One way to overcome this challenge is to increase the surface to a bulk atomic ratio of metal without reducing the metal loading to the material, incorporating non-noble metals to replace or supplement platinum on the photocatalysts.[14]

The CdS semiconductor has the potential to function as a photocatalyst for water splitting reactions due to its suitable band gap, electron affinity, and responsiveness to visible light.[14] However, its photocatalytic activity is limited by photo corrosion and aggregation. To enhance its

performance, different methods such as introducing metal cocatalysts onto CdS, controlling particle size, and attaching CdS with other semiconductors can be employed.[5] The introduction of metal cocatalysts helps to decrease electron-hole recombination and acts as a reaction site for the reduction of water. Research has shown that noble metals like Pt, Pd, Au, Ag, and Rh-loaded onto CdS semiconductors perform better as photocatalysts than bare CdS semiconductors.[19] For instance, loading Pt onto CdS can increase photocatalytic hydrogen production by up to 20 times.[19] A new photocatalyst with low loading of Pt (0.30%) and PdS (0.13%) as cocatalyst to CdS has also been developed, achieving quantum efficiency of up to 93%.[19] Recent efforts have focused on developing low-cost photocatalysts by attaching non-noble metals. For example, CdS nanosphere with NiS quantum dots produces 24 times more hydrogen gas than a pure CdS nanosphere due to the incorporation of NiS quantum dots, which reduces the rate of electron hole recombination by separating photogenerated charge carriers.[20]

Amirav et al designed a metal-semiconductor-semiconductor heterojunction, Pt tipped CdS nanorods with CdSe seed.[22] The metal present in the metal-semiconductor heterojunction facilitates photogenerated charge separation and acts as a reaction site for hydrogen evolution reaction but still faces electron hole recombination. In the new photocatalyst, holes are confined in the CdSe seeds, and electrons reside in the metal. In this system, electrons are separated from holes by three components which limit electron hole recombination (Figure 1.7-A). By controlling the length of CdS and diameter of CdS seed different photocatalyst were synthesized and compared their performance for hydrogen production. It was observed that 70 nm long CdS nanorods perform as a better photocatalyst compared to 27 nm long nanorods when the diameter of the CdSe seed was 3.1 nm (Figure 1.7-B). A similar trend was observed when the

CdSe seed diameter was 2.3 nm with the different lengths of CdS rods. It was reported that photocatalysts with a smaller seed diameter with comparable lengths produce greater amounts of hydrogen than other photocatalysts. CdSe seed with a smaller diameter facilitates charge separation efficiently compared to a larger seed because when the diameter increased band gap will increase and limits the rate of electron hole recombination while longer CdS helps to spatially separate two half reactions of water splitting reaction further apart.

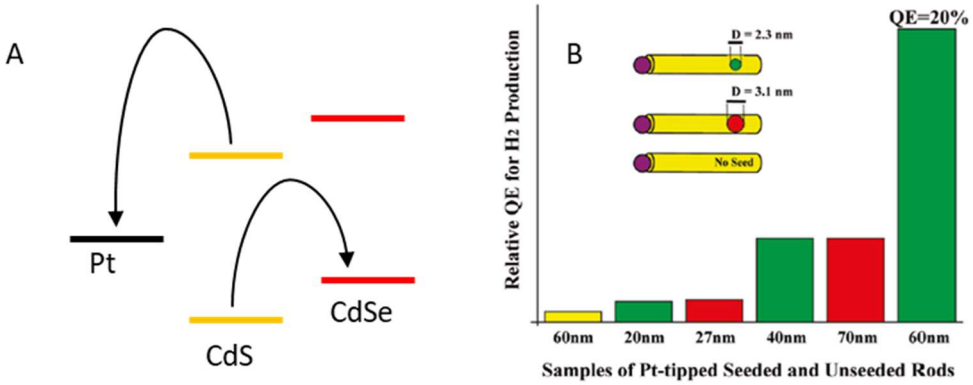

Figure 1.7 A) A schematic representation of charge separation by three component system Pt tipped CdS rod with CdSe seed. B) relative quantum efficiency of hydrogen production for Pt tipped CdS rods without CdSe seed(yellow) and five other samples with different rod lengths and seed diameters. The X-axis represents relative quantum efficiency while the Y-axis represents the average length of the CdS rods. This figure is reproduced from reference 22.

1.3 Overview of research

In our research, we are trying to use the finding of the Suryanto et al paper that Ni-Fe nanoparticles can replace platinum in electrochemical water splitting reactions and apply this idea to photocatalysts that use platinum cocatalysts.[9] Amirav et al developed a photocatalyst, Pt-tipped CdS nanorods with CdSe seed.[22] It was reported that platinum tipped CdS nanorods with

CdSe seed acts as a photocatalyst and produces a greater amount of hydrogen gas compared to bare CdS nanorods due to holes confined into CdSe seed and electrons being transferred to metal and reducing the electron-hole recombination.[7] The presence of seed onto CdS nanorods increases the stability of heterostructure semiconductors by reducing photo erosion.

Our research goal is to replace platinum with iron, nickel, or both on CdSe/CdS nanorods and develop a new photocatalyst for water splitting as shown in Figure 1.8.

In this thesis, we are focused on the synthesis of CdSe/CdS nanorods and metal decoration using two different approaches, reducing metal salts at high temperature (polyol reduction) and photodeposition. First, we synthesized CdSe quantum dots which were then used to synthesize CdSe/CdS nanorods. Synthesis and characterization of CdSe quantum dots and CdSe/CdS nanorods are described in Chapter 3 and Chapter 4 respectively. Then we tried to deposit platinum, iron, and nickel onto CdSe/CdS nanorods by two different methods which are described in Chapter 5. Optical emission spectroscopy and electron microscopy were used to learn about the composition and morphology of different metal decorated nanorods. The complete photocatalyst proposed has not yet been synthesized, and these materials will need further development before conducting photocatalytic water splitting experiments.

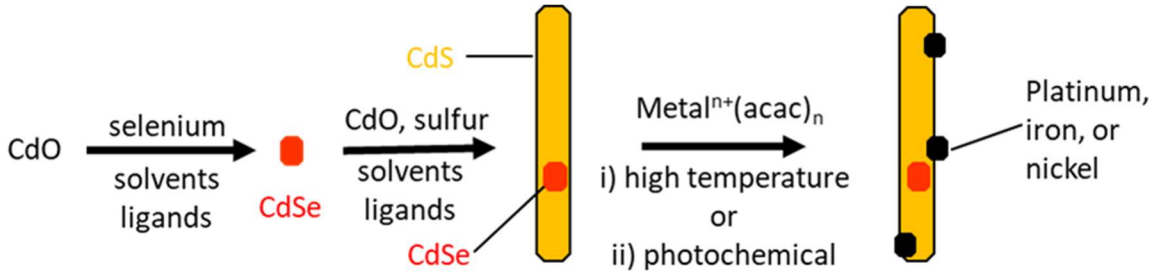

Figure 1.8 Overview of materials described in this thesis. CdSe quantum dots (chapter 3), CdSe/CdS nanorods (chapter 4), and metal co-catalyst semiconductor hybrid photocatalyst which can be achieved by two different synthetic routes (chapter 5).

Chapter 2. Experimental

In this chapter, the procedure for the synthesis of CdSe quantum dots, CdSe/CdS nanorods, and metal deposition onto CdSe/CdS nanorods are described. Materials and instruments which were used in the different experiments are also described in this chapter.

Table 1. Definitions of abbreviations used in this thesis.

Chemicals	**Abbreviations**
octadecylphosphonic acid	ODPA
trioctylphosphine	TOP
trioctylphosphine oxide	TOPO
hexylphosphonic acid	HPA
metal acetylacetonate	$Metal^{n+}(acac)_n$
oleic acid	OLAC
oleylamine	OLAM
1,2-hexadecanediol	HDD
diphenyl ether	DPE
dichlorobenzene	DCB
TEM	Transmission electron microscopy
HAADF	High angle annular dark-field imaging
STEM	Scanning transmission electron microscopy
ICP	Inductively coupled plasma
OES	Optical emission spectroscopy

2.1 Materials

Cadmium oxide, trioctylphosphine oxide, trioctylphosphine, selenium, toluene, octadecene, hexylphosphonic acid, oleic acid, diphenyl ether, 1,2-hexadecanediol, platinum(II) acetylacetonate, nickel(II) acetylacetonate, iron(III) acetylacetonate, oleylamine and 1,2-dichlorobenzene were purchased from Sigma Aldrich and octadecylphosphonic acid was purchased from Synthonix. Calibration standard solutions of cadmium, iron, nickel, and platinum were purchased from Inorganic Ventures. All chemicals were used without further purification.

2.2 Synthesis

2.2.1 Procedure for synthesis of CdSe quantum dots

CdSe quantum dots capped with phosphonic acid ligands were prepared by hot injection as previously reported.[32]

TOP: Se stock solution

A stock solution of selenium dissolved in trioctylphosphine (TOP) was prepared under argon for later use. Selenium powder (1.398 g) was weighed into a 20 mL scintillation vial with a stir bar and sealed tightly with a septum that was secured to the vial with duct tape. The gases in the vial were evacuated under reduced pressure and the headspace was filled with argon (3 cycles) before adding trioctylphosphine (10.0 mL) under an argon atmosphere. The mixture was stirred overnight until the solids dissolved, ensuring that the contents of the vial did not contact the septum.

Cadmium complexation

Cadmium oxide (0.180 g), trioctylphosphine oxide (TOPO) (9.000 g), and octadecylphosphonic acid (ODPA) (0.840 g) were loaded into a three-neck round-bottom flask containing a stir bar, fitted with a reflux condenser and a temperature probe, and the remaining neck was sealed with a septum. Then, the gently stirred mixture was placed under a vacuum and heated to 150 °C for 20 minutes followed by filling the headspace of the flask with argon and the mixture was heated to 300 °C with vigorous stirring and held at this temperature until a clear/colorless solution was observed.

Hot injection of TOP: Se

Trioctylphosphine (5.5 mL) was injected, and the solution was heated to 380 °C. The heating mantle was carefully removed from beneath the flask and the stirring was allowed to stabilize briefly before the trioctylphosphine/selenium stock solution (1.2 mL) was quickly injected into the vigorously stirring mixture under argon. After 12 seconds from the time of injection, 1-octadecene (15.0 mL) was injected slowly to quench the reaction, and toluene (15.0 mL) was added after cooling to approximately 100 °C to prevent the solidification of the mixture at room temperature.

Purification

After cooling to room temperature, the crude product was transferred to two 50 mL centrifuge tubes and each tube was diluted to approximately 48 mL with ethanol to precipitate the particles. The dispersions were centrifuged for 7 minutes at 7000 rpm, and the supernatants were decanted. The pellets were dispersed in 15 mL toluene each, diluted to approximately 48 mL with ethanol, and centrifuged for 7 minutes at 7000 rpm, and supernatants were decanted. The pellets are dispersed in toluene and precipitated with ethanol once more followed by centrifugation as above. The pellets obtained from the third centrifugation cycle were transferred to a tared vial with dichloromethane and then dichloromethane was evaporated under reduced pressure and the resulting solids were dried under vacuum at 60 °C for up to 2 days. The yield of CdSe quantum dots for Sample A and Sample B were 0.098 g and 0.130 g respectively.

2.2.2 Synthesis for the procedure of CdSe/CdS nanorods

The procedure for the growth of CdS shells around the CdSe quantum dots synthesis was adopted from the literature.[23]

TOP:S and CdSe QDs stock solution

The trioctylphosphine (TOP), sulfur, and CdSe quantum dots stock solution were prepared for later use by the addition of elemental sulfur powder (0.500 g) and CdSe quantum dots (0.080 g) in a 20 mL scintillation vial with a stir bar, and then sealing a septum tightly with duct tape, evacuating air, and filling with argon. Trioctylphosphine (TOP) (15 mL) was then injected under argon and the solution was stirred overnight.

Cadmium Complexation

Cadmium oxide (0.32 g), trioctylphosphine oxide (TOP) (12.00 g), octadecylphosphonic acid (ODPA) (1.12 g), and hexylphosphonic acid (HPA) (0.32 g) were loaded into a three-neck round-bottom flask with a stir bar, fitted with a reflux condenser, a temperature probe was connected, and the remaining neck was sealed with a septum. The mixture was then placed under a vacuum and was heated to 150 °C for 30 minutes while stirring at 300 rpm. The headspace of the flask was then filled with argon and the mixture was heated to 320 °C and held at this temperature until the formation of a clear/colorless solution.

Hot injection

Trioctylphosphine (TOP) (7.20 mL) was injected, and the solution was held at 320 °C for an additional 20 minutes. Then the solution was heated to 380 °C and the trioctylphosphine (TOP), sulfur, and CdSe quantum dots stock solution (7.20 mL) was injected quickly, and the temperature was held at approximately 350 °C for 6 minutes before removing the heating mantle. Toluene (20 mL) was then slowly added after cooling to approximately 150 °C to prevent solidification of the mixture at room temperature.

Purification

After cooling to room temperature, the crude product was transferred to four 50 mL centrifuge tubes, each tube was diluted to 27 mL with toluene, and then diluted to approximately 48 mL with ethanol to precipitate the particles. The dispersions were shaken to mix, centrifuged for 7 minutes at 7000 rpm and the supernatants were decanted. The above pellets were dispersed in 22 mL toluene each, diluted to approximately 48 mL with ethanol, shaken to mix, centrifuged for 7 minutes at 7000 rpm, and the supernatants were again decanted. The above pellets were dispersed in 12 mL toluene each, diluted to approximately 48 mL with ethanol, shaken to mix, and centrifuged for 10 minutes at 7000 rpm before the supernatants were decanted. The pellets obtained from the third centrifugation cycle were transferred to a tared vial with dichloromethane and a small (0.1 mL) sample was taken for TEM imaging before the dichloromethane was evaporated from the pellet under reduced pressure and the resulting solids were dried under vacuum at 60 °C for up to 2 days. The yield of CdSe/CdS nanorods was 0.077 g and 0.155 g respectively for Sample A and Sample B synthesis experiments. The small aliquot taken for TEM was dispersed in toluene (1.0 mL) in a small vial and cast onto a TEM grid.

2.2.3 Procedure using polyol reduction for metal decoration onto CdSe/CdS nanorods

The synthesis procedure for platinum decoration onto CdSe/CdS by polyol reduction was reported previously.[24] This procedure was applied to iron and nickel as described below.

Reducing agent and solvent

Oleic acid (OLAC, 0.1 mL), oleylamine (OLAM, 0.1 mL), 1,2-hexadecanediol (HDD, 0.021 g), and diphenyl ether (DPE, 5.0 mL) were loaded into a 50 mL three-neck-round bottom equipped with

a reflux condenser and 1-inch stir bar. The reaction mixture was then heated to 80 °C under vacuum for 30 min at 300 RPM using a heating mantle.

Metal precursor and nanorods dispersion

Metal acetylacetonate ($metal^{n+}(acac)_n$, 0.031 mmol as metal) and CdSe/CdS nanorods (0.012 g) were added to a 20 mL vial and dispersed in 1,2-dichlorobenzene (DCB, 1.5 mL) by vortex mixing followed by sonication for at least 30 minutes just before injection.

Hot injection

The reaction mixture was then heated to 225 °C under argon before injecting the platinum precursor and nanorods dispersion, and the reaction mixture was maintained at 225°C under argon gas flow for 8 minutes. After 8 minutes the reaction had turned completely black and was removed from the heating mantle. Toluene (10.0 mL) was injected upon cooling to below 100°C.

Purification

The crude sample was transferred to a centrifuge tube (50 mL) and diluted to 35 mL with toluene. The solution was precipitated with the addition of ethanol (10.0 mL). Then the solution was centrifuged at 2500 rpm for 12 minutes. The supernatant was decanted, and the pellet was dispersed in toluene (35.0 mL) before adding ethanol (10.0 mL) to the centrifuge tube. Then the solution was centrifuged again at 2500 rpm for 12 minutes. The pellet was transferred to a tared vial using dichloromethane and a small (0.1 mL) sample was taken for TEM imaging before the dichloromethane was evaporated from the pellet under reduced pressure and the resulting solids were dried under vacuum at 55 °C overnight. The small aliquot taken for TEM was dispersed in toluene (1.0 mL) in a small vial and cast onto a TEM grid.

2.2.4 Procedure for photodeposition of metals onto CdSe/CdS nanorods

The synthesis procedure of platinum decoration via photodeposition was reported previously,[25,26] and this procedure was applied to iron and nickel as described below.

CdSe/CdS nanorods and metal precursor solution

CdSe/CdS nanorods (0.005 g) were dispersed in toluene (4.5 mL) containing triethylamine (0.5 mL) and metal acetylacetonate ($metal^{n+}(acac)_n$, 0.038 mmol as metal) in a photocatalytic reaction cell with a stir bar. Then the solution was sparged with nitrogen gas for 15 minutes.

Light irradiation

The reaction cell was sealed with a lid and irradiated with a xenon arc lamp and placed directly in contact with the reaction cell for four hours with continuous stirring at 300 rpm.

Purification

The solution was divided between two 15 mL centrifuge tubes and each tube was diluted to 15 mL with ethanol. Centrifugation at 2500 rpm for 12 minutes afforded a black pellet which was retained and a clear supernatant which was discarded. The pellets were dispersed in toluene and precipitated with ethanol followed by centrifugation as above. The pellets obtained after four centrifugation cycles are dispersed in toluene and stored in a 20 mL sealed vial.

2.2 UV-vis spectroscopy

A Shimadzu UV-2600 UV-vis spectrophotometer was used to obtain UV-vis spectra. The samples were scanned with a wavelength range of 300 nm to 800 nm when the slit width was 2 nm. The spectrophotometer was set to its slowest speed with 2 nm increments using absorbance

measuring mode, and samples were held in a 0.5 mL quartz cuvette. The spectrometer was blanked using toluene and samples were dispersed in toluene.

2.3 Fluorescence spectroscopy

A PerkinElmer FL 6500 fluorescence spectrophotometer was used to get the emission spectrum. The instrument was operated at 100 Hz frequency when the slit width was 5 nm. Emission spectra were collected by using fluorescence light source mode. Samples were held in a 0.5 mL quartz cuvette. An excitation wavelength was selected for each sample and scanned with a wavelength range of 300 nm to 900 nm depending on which excitation wavelength was used for the sample. Toluene was used for background correction of the instrument. All samples were dispersed in toluene and then emission spectra were collected.

2.4 Transmission electron microscope (WKU)

A JEOL 1400Plus transmission electron microscope was used to image synthesized particles for TEM imaging. A voltage setting of 100kv was used for imaging. The magnification of the images ranged from 100x to 250000x. A lanthanum hexaboride (LaB6) filament was used. AMT camera engine software was used to collect images of the sample.

Two different types of TEM grids were used for TEM imaging. The tabbed center-marked grids with 200 mesh, and 3.0mm O.D with copper support were purchased from Ted Pella. Carbon-coated mica was collected from WKU Electron Microscopy Lab. A small portion of mica cut which was approximately the same size as the TEM grids. Then it was placed on a droplet of water. It was found a thin film of carbon floated on the water droplet when mica sank to the bottom of the water because mica is hydrophilic, and carbon is hydrophobic. The copper grid was placed

into the water droplet and under the carbon film. Then the copper grid was lifted with carbon film so that the surface of the grid became carbon coated. The copper grid was placed on filter paper to dry before samples were cast onto the grid. Another type of TEM grid was used which was a lacey carbon grid with 300 mesh, and grid hole size: 63µm copper supported purchased from Ted Pella. Samples were dried at 100 overnight under a vacuum to evaporate toluene.

ImageJ software was used to measure the average length and diameter of the CdSe quantum dots, CdSe/CdS nanorods, and different metal decorated nanorods.[27] Size distributions were determined by measuring the dimensions of at least 100 particles for each sample.

2.5 Transmission electron microscope (UK)

A Thermo Scientific™ Talos™ F200X TEM operating at 200 kV accelerating voltage equipped with a 16M pixel 4k x 4k CMOS camera was used to collect HAADF and EDS images. TEM grid was used which was a lacey carbon grid with 300 mesh, and grid hole size: 63µm copper supported purchased from Ted Pella. The sample which was dispersed in toluene cast onto the lacey carbon grid and was dried at 100 overnight under vacuum to evaporate toluene.

2.6 Inductively coupled plasma-optical emission spectroscopy

A ThermoScientific ICAP 6500 ICP-OES was used to determine the concentration of different metals in the sample. A series of standard solutions were prepared to produce standard calibration curves for metal contraction determination. Calibration standard solutions containing cadmium, iron, and nickel were prepared by diluting a 1000 ppm standard solution. Five different calibration standards solutions (50 mL) were prepared with nitric acid (10% v/v) as a diluting solution (1.0 ppm, 2.5 ppm, 5 ppm, 7.5 ppm, and 10 ppm). This set of calibration

standard solutions was used to determine the concentration of cadmium, iron, and nickel in the sample.

A small spatula tip amount of purified nanorods were dispersed into toluene. Then CdSe/CdS nanorods (1.00 mL) and metal deposited CdSe/CdS nanorods (1.00 mL) were transferred into a vial (20 mL) which were dispersed in toluene. Samples were dried at 100 °C overnight under a vacuum to evaporate toluene from the samples. After evaporating toluene from the sample, concentrated hydrochloric acid (0.9 mL) and concentrated nitic acid (0.3 mL) were added to the sample for digestion and diluted to 10 mL with nitric acid (10 % v/v) solution. The nitric acid (10 % v/v) solution was used as a blank solution. Then ICP-OES data were collected for bare nanorods and different metal decorated nanorods.

2.7 Centrifugation

In 50-mL polypropylene centrifuge tubes from VWR, samples were centrifuged using a Thermo Scientific Sorvall ST 8 with a radius of 12 cm (max rcf 17,000 g).

Chapter 3. CdSe quantum dots

In our research, we synthesized two different batches of CdSe/CdS nanorods from two different batches of CdSe quantum dots. In this chapter, these two batches of CdSe quantum dots are described as Sample A and Sample B.

The reaction scheme of the synthesis of CdSe quantum dots is shown below in Figure 3.1. CdSe quantum dots were synthesized from cadmium and selenium precursors in the presence of trioctylphosphine oxide (TOPO) and trioctylphosphine (TOP) and octadecylphosphonic acid (ODPA). The properties of CdSe quantum dots largely depend on the size of the quantum dots. Ligands like octadecylphosphonic acid (ODPA) help to stabilize the growth of quantum dots and prevent the aggregation of nanocrystals. CdSe quantum dots synthesis is the first step of synthesis of the core/shell structure of CdSe/CdS nanorods which is described in Chapter 4.

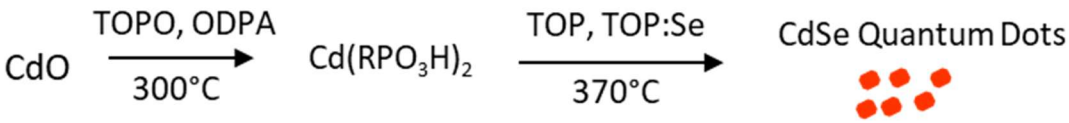

Figure 3.1 Reaction scheme for the synthesis of CdSe quantum dots.

3.2 Characterization

3.2.1 UV-Vis and fluorescence spectroscopy

When the size of the quantum dots becomes smaller the band gap becomes larger compared to the larger quantum dots. It was reported that there is a correlation between the size of the quantum dots and the lowest energy absorption peak of UV-vis absorption spectra, and the following equation (1) was empirically determined by relating the average size of CdSe quantum dots with the lowest energy absorption wavelength.[28]

$$\text{CdSe: } D = (1.6122 \times 10^{-9})\lambda^4 - (2.6575 \times 10^{-6})\lambda^3 + (1.6242 \times 10^{-3})\lambda^2 - (0.4277)\lambda + (41.57) \quad (1)$$

D is the diameter (nm) of the CdSe quantum dots and λ (nm) is the wavelength of the lowest energy absorption peak. Many samples of quantum dots were used to obtain this correlation, where all the quantum dots were synthesized using the same reagents and reaction temperature. This correlation has since been used in the literature to benchmark sizes of CdSe quantum dots prepared by various methods with mixed results.

Sample A shows a UV-vis absorption peak (Figure 3.2-A, black solid line) at approximately 574 nm while Sample B shows at approximately 608 nm (Figure 3.2-B, black solid line). Equation (1) was used to estimate the diameter of CdSe quantum dots for Sample A and Sample B as 3.57 nm and 5.27 nm respectively.

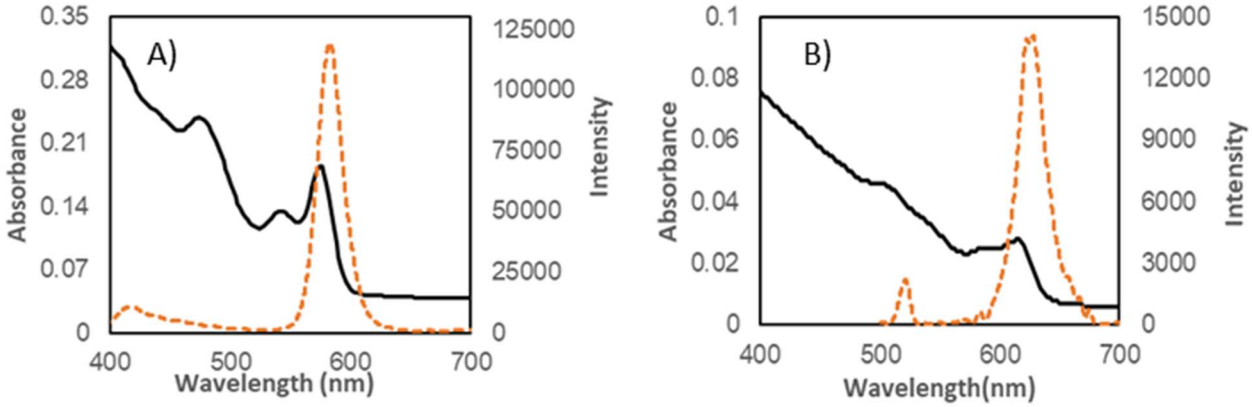

Figure 3.2 Absorption (black solid line, left y-axis) and fluorescence emission spectra (orange dotted line, right y-axis) of CdSe quantum dots. The lowest energy absorbance peak for A) Sample A and B) Sample B was observed at 574 nm and 608 nm respectively. Emission peaks were observed at 584 nm for Sample A and 629 nm for Sample B. Excitation wavelengths for Sample A and Sample B were 400 nm and 450 nm, respectively.

Figure 3.2 shows the absorption spectra and fluorescence emission spectra of CdSe quantum dots. Sample A was excited at 400 nm wavelength and shows emission peaks at 584 nm (Figure 3.2-A, orange dotted line) while Sample B was excited at 450 nm wavelength and shows emission

peaks at 523 nm and 629 nm (Figure 3.2-B, orange dotted line). The fluorescence emission wavelength is slightly red shifted from the absorption peak, as expected for these materials.[28]

3.2.2 Transmission electron microscopy (TEM)

Figure 3.3 shows the TEM images of CdSe quantum dots. Quantum dots in both samples were not spherical (prolate spheroids), with the average lengths and diameters of CdSe quantum dots of Sample A measured as 5.3 ± 1.0 nm and 3.1 ± 0.6 nm respectively (Figure 3.3-A) while the average length and diameter of CdSe quantum dots of Sample B are 8.0 ± 0.8 nm and 3.7 ± 0.7 nm respectively (Figure 3.3-B) from the TEM images.

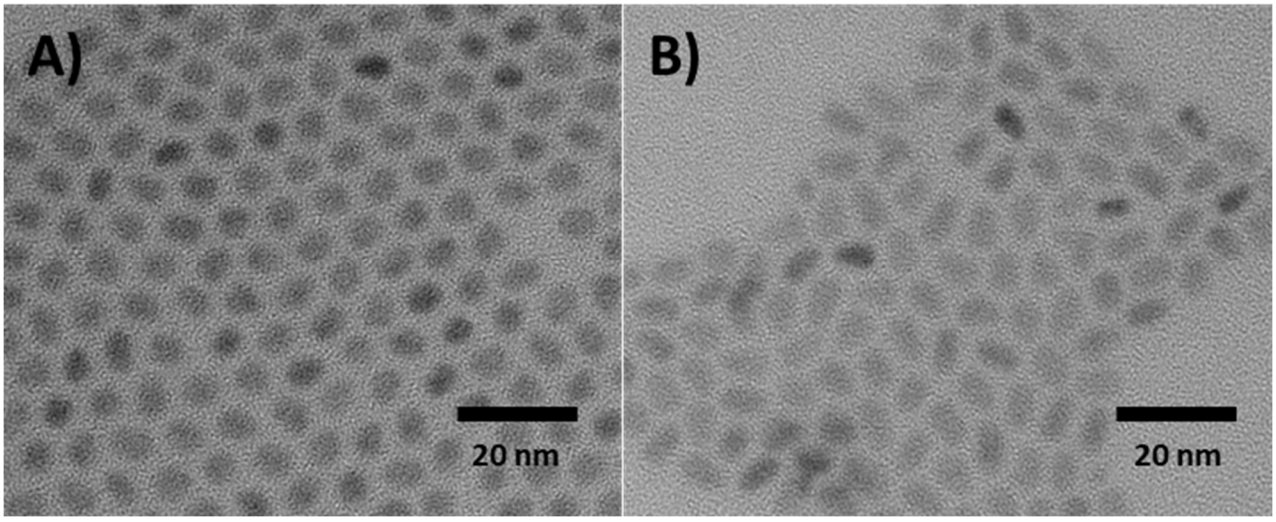

Figure 3.3. TEM images of CdSe quantum dots showing the average length and diameter of A) Sample A are 5.3 ± 1.0 nm and 3.1 ± 0.6 nm respectively whereas the average length and diameter of CdSe quantum dots of B) Sample B are 8.0 ± 0.8 nm and 3.7 ± 0.7 nm respectively. The diameter was measured using ImageJ software.[27]

3.3 Discussion

Sample A CdSe quantum dots show absorbance at 574 nm (Figure 3.2-A, black solid line) with emission spectra slightly red shifted at 584 nm (Figure 3.2-A, orange dotted line). This phenomenon also was observed for Sample B CdSe quantum dots where absorbance was

observed at 608 nm (Figure 3.2-B, black solid line) and emission at 629 nm (Figure 3.2-B, orange dotted line). It was also observed that there is a significant deviation between the average diameter estimated using UV-Vis lowest energy wavelength correlation (equation 1) versus measurements obtained by sizing TEM images (Table 2). This discrepancy between estimated and measured diameters has been seen before,[10] and can be partially attributed to using a different synthesis procedure and capping ligands than the study which initially reported the correlation of UV-vis absorbance with diameter.

Table 2. Comparison of different properties of Sample A and Sample B CdSe quantum dots.

	Absorbance (nm)	Emission (nm)	Estimated diameter from UV-vis (nm)	Measured length from TEM (nm)	Measured diameter from TEM (nm)
Sample A	574	584	3.57	5.3 ± 1.0	3.1 ± 0.6
Sample B	608	629	5.27	8.0 ± 0.8	3.7 ± 0.7

These two batches of CdSe quantum dots were used to synthesize two different batches of CdSe/CdS nanorods.

Chapter 4. CdSe/CdS core/shell nanorods

Our goal is to deposit different metals (Pt, Fe, and Ni) deposited onto nanorods to compare these materials as photocatalysts. However, these nanorods are obtained in small batch sizes, so we needed two batches of nanorods (Sample A and Sample B) to study the different metal deposition conditions described in Chapter 5.

Figure 4.1 shows the reaction scheme for the synthesis of CdSe/CdS nanorods. CdS shell grows around CdSe quantum dots to get the core/shell CdSe/CdS nanorods which are the photosensitizer portion of the photocatalyst that harvests sunlight. Electron hole recombination decreases photocatalytic activity in pure semiconductors, and the core/shell structure minimizes the rate of electron-hole recombination. Organic ligands with electron-donating groups like octadecylphosphonic acid (ODPA) and hexadecylphosphonic acid (HPA) help to foster shell growth around the core.

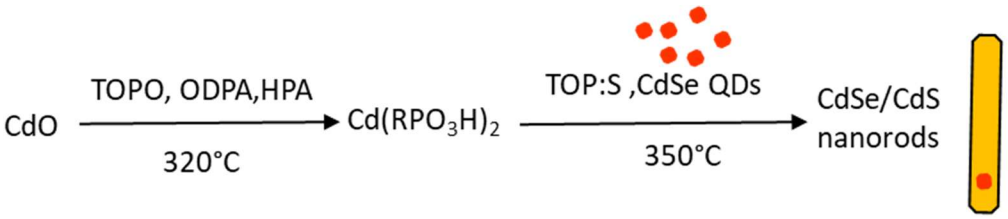

Figure 4.1 Reaction scheme for the synthesis of CdSe/CdS nanorods.

4.2 Characterization

4.2.1 UV-Vis and fluorescence spectroscopy

Figure 4.2 shows the absorption (black solid line) and emission spectra (orange dotted line) of CdSe/CdS nanorods. The absorption spectra can in principle include features from the CdSe seed, the CdS shell, and the CdSe/CdS interface (heterojunction). Sample A (Figure 4.2-A, black solid line) shows an absorption shoulder attributed to CdS at 471 nm while Sample B (Figure 4.2-B,

black solid line) shows a similar shoulder at 474 nm. Absorption features attributed to the CdSe seed were not observed in either sample. An absorbance feature at 611 nm attributed to the CdSe/CdS heterojunction was observed for sample A (Figure 4.2-A, dotted grey line), while a similar feature was not conclusively observed for sample B (Figure 4.2-B, dotted grey line).

Sample A shows an emission peak at 603 nm (Figure 4.2-A, orange dotted line) when the excitation wavelength was 500 nm while Sample B shows an emission peak at 662 nm (Figure 4.2-B, orange dotted line) when the excitation wavelength was 550 nm.

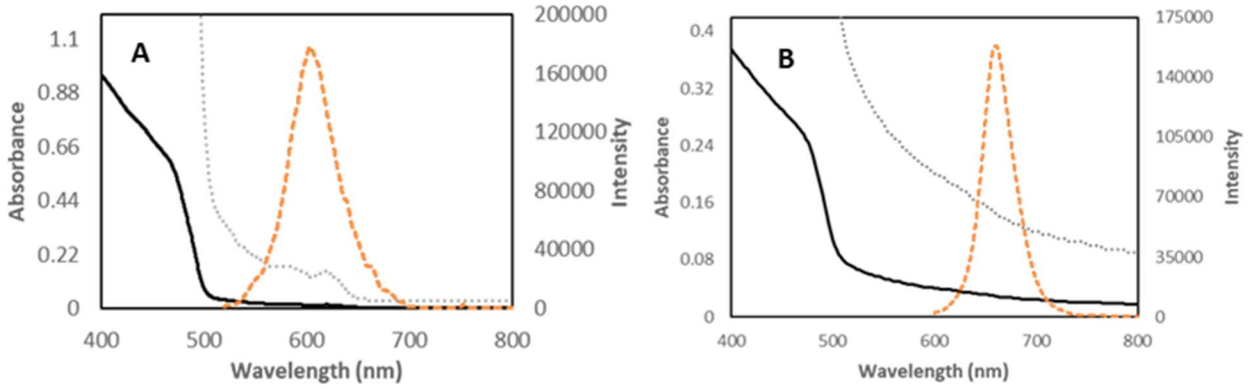

Figure 4.2 UV-vis absorption (left y-axis, black solid line, and dotted gray line) and fluorescence emission spectra (right y-axis, orange dotted line) of CdSe/CdS nanorods. Absorbance peak at 471 nm was observed for A) Sample A and at 474 nm for B) Sample B. A shoulder peak was observed at 611 nm (Figure 4.2-A, dotted grey line) for Sample A, but this absorption peak was not observed in Sample B. Emission peaks were observed at 603 nm for Sample A and 662 nm for Sample B. Excitation wavelengths for sample A was at 500 nm while for Sample B at 550 nm.

4.2.2 Transmission electron microscopy

Figure 4.3 shows TEM images of core/shell CdSe/CdS nanorods of Sample A (Figure 4.3-A and Figure 4.3-C) and Sample B (Figure 4.3-B and Figure 4.3-D). The average length and diameter of CdSe/CdS nanorods were 98.3 ± 7.2 nm and 2.8 ± 0.5 nm for Sample A, respectively while the average length and diameter of CdSe/CdS nanorods were 29.7 ± 2.6 nm and 7.0 ± 1.2 nm for Sample B, respectively. The length and diameter of CdSe/CdS nanorods were measured by using ImageJ software.[14]

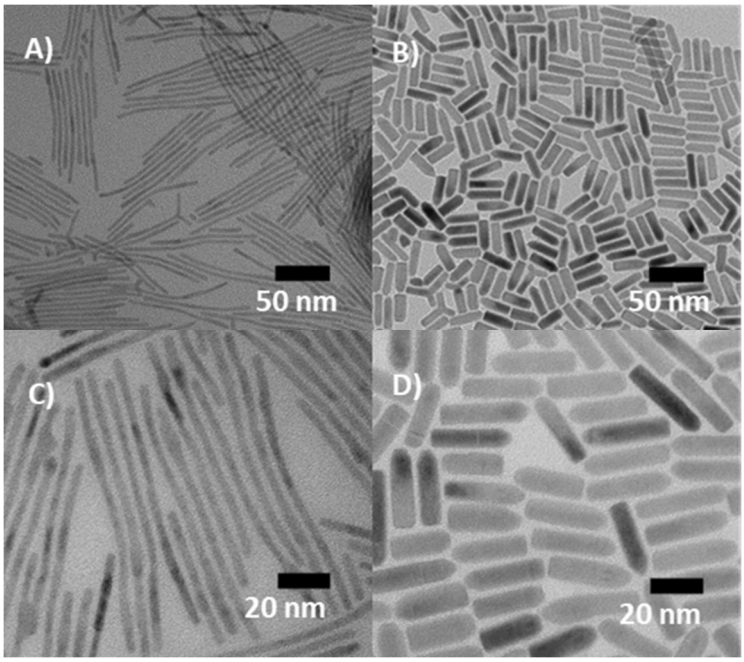

Figure 4.3 TEM images of Sample A (A-low magnification, C-high magnification) and Sample B (B-low magnification, D-high magnification) CdSe/CdS nanorods. All images were taken at 100 KV. The average length and diameter of CdSe/CdS nanorods were 98.3 ± 7.2 nm and 2.8 ± 0.5 nm for Sample A while the average length and diameter of CdSe/CdS nanorods were 29.7 ± 2.5 nm and 7.0 ± 1.2 nm for Sample B. The length and diameter of nanorods were measured by using ImageJ software.[14]

4.3 Discussion

Two different batches of quantum dots were used to synthesize two different batches of CdSe/CdS nanorods. The average length and diameter of the two batches of nanorods were different due to the presence of different CdSe seeds in the nanorods (Table 3). A small absorbance feature at approximately 611 nm (Figure 4.2-A, dotted grey line) was observed for Sample A CdSe/CdS nanorods which were not observed for Sample B nanorods (Figure 4.2-B, dotted grey line). This shoulder peak is attributed to light absorption by interfacial states associated with the core/shell structure.[31] Sample A (Figure 4.3-A and C) nanorods are thinner compared to Sample B (Figure 4.3-B and D) nanorods, and due to this light can be absorbed at the interface of the core/shell of Sample A and shoulder peak at 611 nm was observed. Nanorods

are thicker for Sample B, and due to the greater thickness light absorption is not observed at the interface of the core /shell of Sample B. However, strong emission peaks were observed for both Sample A (Figure 4.2-A, orange dotted line) and Sample B (Figure 4.2-B, orange dotted line) CdSe/CdS nanorods, which is evidence for the core/shell heterojunction in both materials.

Table 3. Comparison of different properties of Sample A and Sample B CdSe/CdS nanorods.

	Absorbance (nm)	Ex. Wavelength (nm)	Emission (nm)	Nanorod length from TEM (nm)	Nanorod diameter from TEM (nm)	Quantum dot seed diameter from TEM (nm)
Sample A	471	500	603	98.3 ± 7.2	2.8 ± 0.5	3.1 ± 0.6
Sample B	474	550	664	29.7 ± 2.5	7.0 ± 1.3	3.8 ± 0.7

These two different batches of CdSe/CdS nanorods were used for the synthesis of metal decorated nanorods by using reducing metal salts at high temperatures (polyol reduction) and photodeposition methods. Nanorod size and shape vary from batch to batch, and therefore nanorods taken from the same batch were used to evaluate a given approach for metal deposition described in Chapter 5.

Chapter 5. Metal deposition

In our research platinum(II) acetylacetonate, iron(III) acetylacetonate, and nickel(II) acetylacetonate were used as platinum, iron, and nickel sources to synthesize different metal decorated nanorods. We evaluated two different synthetic routes that were previously reported to attach platinum to CdSe/CdS nanorods to determine if these approaches would work for iron and nickel (Figure 5.1). One approach was to reduce the metal salts at high temperatures in the presence of organic reducing agents (the polyol reduction),[24] and the other approach used illumination for photodeposition of metal onto CdSe/CdS nanorods near room temperature.[26]

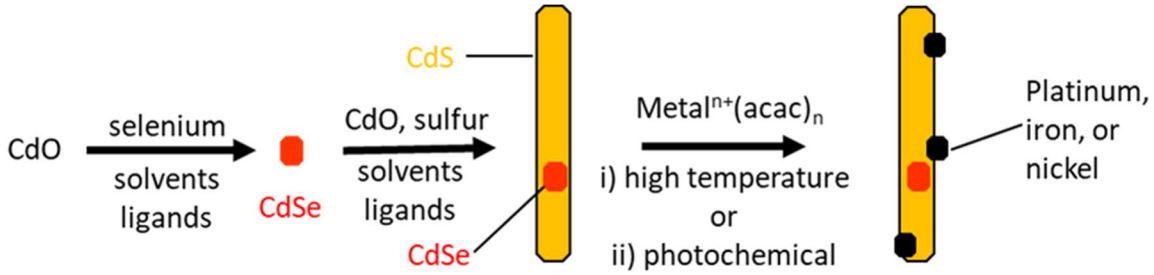

Figure 5.1 Overview of two synthetic routes to achieve metal attached CdSe/CdS nanorods.

5.1 Polyol reduction for metal decoration onto CdSe/CdS nanorods

A reaction scheme for polyol reduction synthesis of metal decorated CdSe/CdS nanorods is shown in Figure 5.2, and the detailed synthesis procedure for metal decoration onto CdSe/CdS nanorods was described in Chapter 2. Metal acetylacetonate (metal^{n+}(acac)$_n$) acts as a metal precursor for the synthesis of metal decorated CdSe/CdS nanorods. Metal acetylacetonate (metal^{n+}(acac)$_n$) and CdSe/CdS nanorods were introduced into the reaction in the presence of oleic acid (OLAC), oleylamine (OLAM), 1,2-hexadecanediol (HDD) and diphenyl ether (DPE). Oleic

acid (OLAC) and oleylamine (OLAM) are used as ligands, and 1,2-hexadecanediol (HDD) acts as a reducing agent to reduce metal precursor to metal and diphenyl ether (DPE) as the solvent.

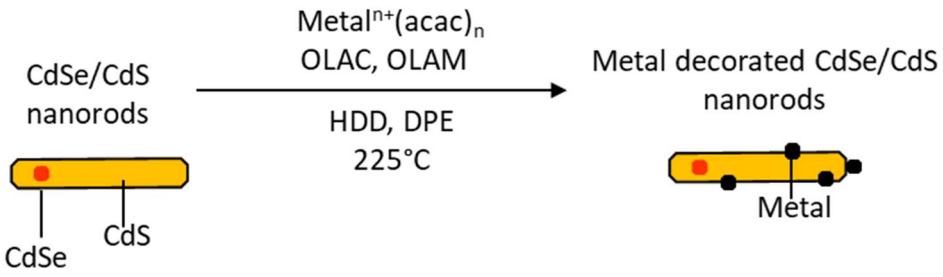

Figure 5.2 Reaction scheme for polyol reduction synthesis of metal decorated CdSe/CdS nanorods.

5.1.1 Transmission electron microscopy from polyol reduction

Figure 5.3 shows TEM images of platinum (Figure 5.3-A), iron (Figure 5.3-B), and nickel (Figure 5.3-C) decorated CdSe/CdS nanorods. High contrast black features are seen clearly from the TEM images after the reduction of platinum in the presence of CdSe/CdS nanorods, but nickel and iron deposition could not be conclusively confirmed using bright-field TEM. The average length and diameter of nanorods were unchanged after metal deposition reactions for each sample.

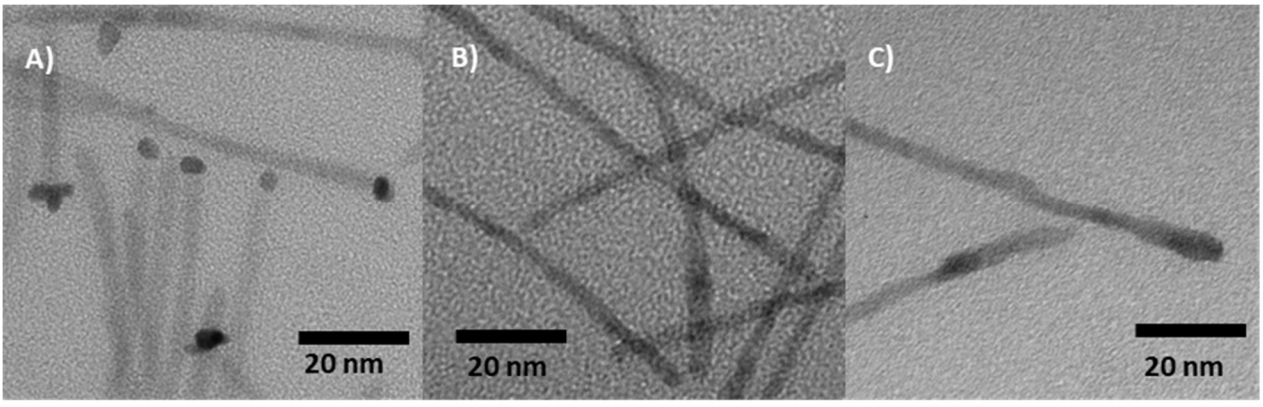

Figure 5.3 TEM images of platinum (Figure 5.3-A), iron (Figure 5.3-B), and nickel (Figure 5.3-C) onto CdSe/CdS nanorods. Platinum decoration onto CdSe/CdS nanorods was observed clearly from bright TEM images but iron and nickel decoration were not confirmed conclusively.

More sensitive microscopy experiments were conducted at the University of Kentucky Electron Microscopy Centre to search for evidence of metal deposition onto these nanorods. High-angle annular dark-field imaging (HAADF) is a technique where detected electrons are incoherently scattered electrons where electrons are scattered at high angles and collected only scattered electrons by an annular detector.[29] HAADF is dependent on the atomic number of the sample and insensitive to sample structure. A sample with a high atomic number will scatter more electrons at higher angles because larger interaction between the nucleus and electron beam due to this a greater signal will record for the sample with a higher atomic number and produce a brighter image of the sample. HAADF is helpful to learn about metal presence and distribution onto heterogeneous material.[29]

We were able to get clear images for platinum decorated CdSe/CdS nanorods but not for iron and nickel decorated nanorods. Iron and nickel are in low contrast compared to platinum, maybe due to this we were unable to see the presence of iron and nickel onto our nanorods. We tried to get better images by changing the sample preparation method. The sample was cast onto lacy carbon supported with copper and dried in a vacuum oven at 100°C overnight to get rid of toluene from the sample. We also tried with different sample holders to get clear images of the samples but still, it was hard to see the presence of metal onto nanorods. We also observed that our nanorods were degraded with the time being under electron beam exposure.

Figure 5.4 shows HAADF images of platinum decorated CdSe/CdS nanorods at low and high magnification. From dark field TEM images, it was seen high contrast dot and a region with low

contrast. The high contrast bright dots represent platinum, and the low contrast region represents CdSe/CdS nanorods.

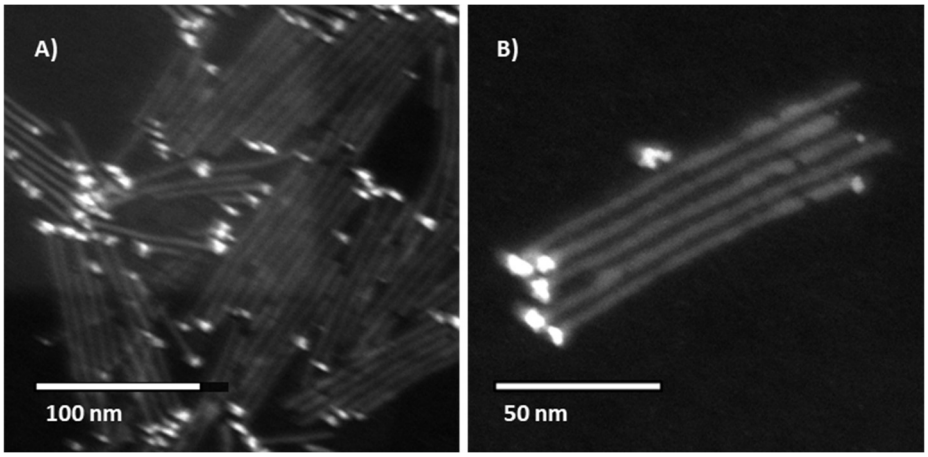

Figure 5.4 HAADF images of platinum decorated CdSe/CdS nanorods at low (Figure 5.4-A) and high magnification (Figure 5.4-B). The images were taken at 200 KV.

Recently we got elemental mapping for iron decorated CdSe/CdS nanorods (Figure 5.5) by using scanning transmission electron microscopy (STEM) with energy dispersive X-ray spectroscopy (EDS). The analytical method of energy-dispersive X-ray spectroscopy (EDS) enables us to know the chemical characterization and elemental analysis of the material.[30] A material that has been activated by an energy source like the electron beam of an electron microscope releases a core electron and a higher energy outer-shell electron moves in to take its place. The difference in energy is subsequently released as an X-ray with a distinctive spectrum depending on its parent atom. An energy dispersive spectrometer is used to collect the number and energy of the X-rays emitted from the sample. The difference in energy between the two shells is characteristic of the element. Each element has a characteristic set of peaks on its electromagnetic emission spectrum. The location of the signal identifies the element while signal strength helps to know the concentration.

The EDS mapping shows the elemental composition of iron decorated CdSe/CdS nanorods (Figure 5.5-A). The green and purple color images represent cadmium (Figure 5.5-B) and iron (Figure 5.5-C) presence onto nanorods.

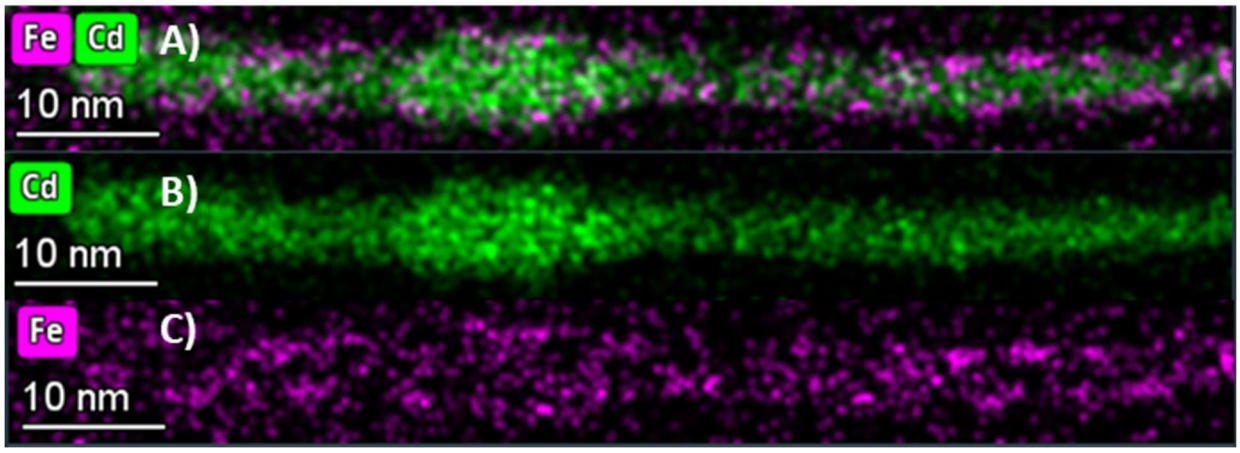

Figure 5.5 shows the EDS mapping of iron decorated CdSe/CdS nanorods. The overlapping image shows iron decoration over CdSe/CdS nanorods (Figure 5.5-A). The green and purple colors represent cadmium (Figure 5.5-B) and iron (Figure 5.5-C) respectively.

5.1.2 Inductively coupled plasma optical emission spectroscopy from polyol reduction

Calibration standard solutions containing cadmium, iron, and nickel were prepared by diluting a 1000 ppm standard solution. Five different calibration standards solutions (50 mL) were prepared with nitric acid (10% v/v) as diluting solution (1.0 ppm, 2.5 ppm, 5 ppm, 7.5 ppm, and 10 ppm). Figure 5.6 shows the standard calibration curve of cadmium, iron, and nickel. This set of calibration standard curves was used to determine the concentration of cadmium, iron, and nickel in the sample. The metal concentration was determined for bare CdSe/CdS nanorods and different metal (platinum, iron, and nickel) decorated CdSe/CdS nanorods. Table 4 represents the concentration of metal and the ratio of cadmium to metal in different metal decorated CdSe/CdS nanorods.

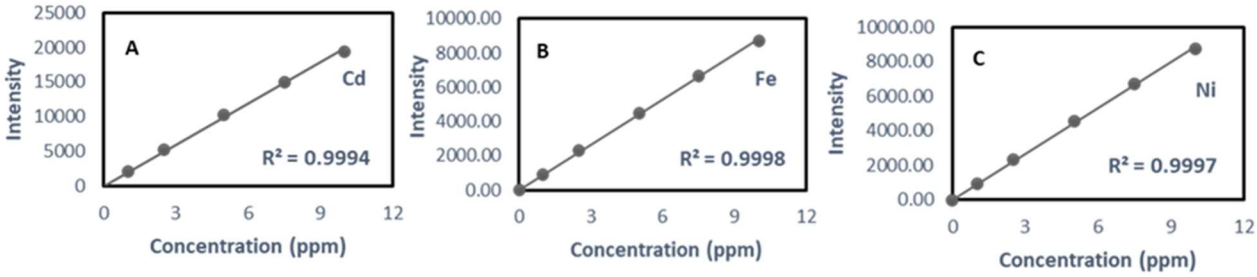

Figure 5.6 standard calibration curves of cadmium (Figure 5.6-A), iron (Figure 5.6-B), and nickel (Figure 5.6-C) for determination of metal concentration present onto different metal decorated CdSe/CdS nanorods and bare CdSe/CdS nanorods.

Table 4. Cadmium, iron, and nickel concentrations obtained from ICP-OES digestion solutions, and the ratio of cadmium to metal onto metal decorated nanorods synthesis via polyol reduction.

Sample	Cd (ppm)	Fe (ppm)	Ni (ppm)	Fe: Cd	Ni: Cd
CdSe/CdS Nanorods	8.05	0.00	0.00	0	0
Fe-CdSe/CdS Nanorods	2.82	0.13	0.00	0.05	0
Ni-CdSe/CdS Nanorods	3.80	0.04	0.29	0.01	0.07

5.1.3 Discussion for polyol deposition of metals onto CdSe/CdS nanorods

Metal decorated CdSe/CdS nanorods were synthesized by reducing metal acetylacetonate salt to metal at high temperatures. The reduced metal can be deposited onto the nanorods or form free metal nanoparticles. Platinum decoration onto nanorods was confirmed from TEM (Figure 5.3-A) and HAADF (Figure 5.4) images but iron and nickel decoration onto nanorods could not confirm conclusively using bright field TEM (Figure 5.3-B and Figure 5.3-C). The concentration of cadmium, iron, and nickel present in nanorods was measured by conducting ICP-OES analysis. We also observed false signals for nickel decorated nanorods. The false signals are negligible to metal concentration. Maybe false signals are coming from the background of the instrument. The ratio of iron to cadmium for iron decorated CdSe/CdS nanorods is 0.05 while the ratio of nickel

to cadmium is 0.29 for nickel decorated nanorods (Table 4). This ICP-OES data determined the concentration of metals in the composite sample, but the location or chemical state of the metals is not confirmed by the ICP-OES.

We observe many free platinum particles in the crude mixture obtained from platinum decoration onto nanorods, and some of these free platinum particles remain after purification. Further, unreduced $Pt(acac)_2$ may be present as platinum ions which would also contribute to the ICP-OES signal. This same incident may happen for iron or nickel decorated nanorods experiments. The signals of iron and nickel were determined by ICP-OES may be coming from free metal or metal ions present in our sample. So, this ICP-OES data gives us information about the presence of metal in the sample but not the metal decoration onto nanorods conclusively. We changed the amount of metal precursor in our reaction scheme six times than the amount of metal precursor mentioned in the synthesis procedure for iron and nickel deposition onto CdSe/CdS nanorods (Chapter 2) and run the reaction for an hour instead of 12 minutes to make nanorods larger and easy to see in TEM images but still, we did not see metal decoration from bright field TEM images for iron and nickel deposition. However, EDS mapping (Figure 5.) provides evidence that at least some iron is deposited onto the nanorod surface, and these materials could be investigated for subsequent deposition of nickel to form the Ni-Fe_xO_y cocatalysts on the nanorod surface. EDS mapping is challenging due to the beam sensitivity of these nanorods, and we have not obtained high quality EDS maps for the nanorods after nickel deposition.

5.2 Photodeposition of metals onto CdSe/CdS nanorods

Photodeposition is one of the ways to synthesize metal decorated nanomaterials. The synthesis procedure for metal photodeposition onto CdSe/CdS nanorods is described in Chapter 2. In this method, the sample is illuminated to generate excited electrons that reduce metal salts to metals at the nanorod surface, with triethylamine acting as a mild sacrificial reducing agent. The photodeposition method is based on the band gap of the semiconductor material. The energy of the photon generated from irradiated light should be greater than the band gap of the semiconductor. Electrons are moved from the valence band to the conduction band when enough energy is absorbed by semiconductors. The reduction potential of the metal ion is needed to be more positive than the conduction band energy of the semiconductor. The semiconductor nanomaterials have large specific surface areas and metal deposition occurs on the surface of the semiconductors. In our research metal acetylacetonate acts as metal precursors and is deposited as metal on the surface of the CdSe/CdS nanorods. The reaction scheme for metal photodeposition onto CdSe/CdS nanorods is shown in Figure 5.7.

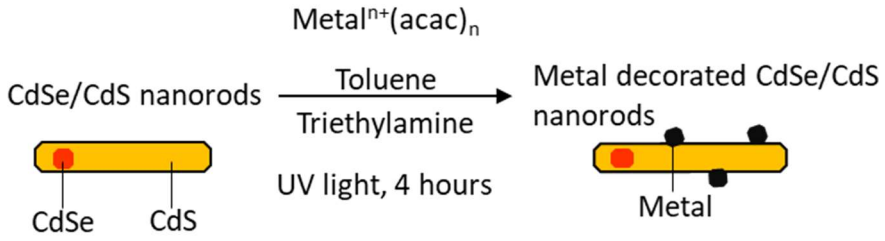

Figure 5.7 Reaction scheme for metal photodeposition onto CdSe/CdS nanorods

5.2.1 Transmission electron microscopy from photodeposition

Figure 5.8 shows bright-field TEM images after the photodeposition of platinum (Figure 5.8-A), iron (Figure 5.8-B), and nickel (Figure 5.8-C) onto CdSe/CdS nanorods. It is seen with high contrast black dots and low contrast regions from bright field TEM images. Those black dots are platinum attached with CdSe/CdS nanorods. Some changes to the nanorod surface were observed for nickel and iron, but nickel and iron nanoparticles attached to CdSe/CdS nanorods could not be conclusively identified or measured using bright-field TEM at 100 kV. The average length and diameter of nanorods were statistically unchanged after metal deposition.

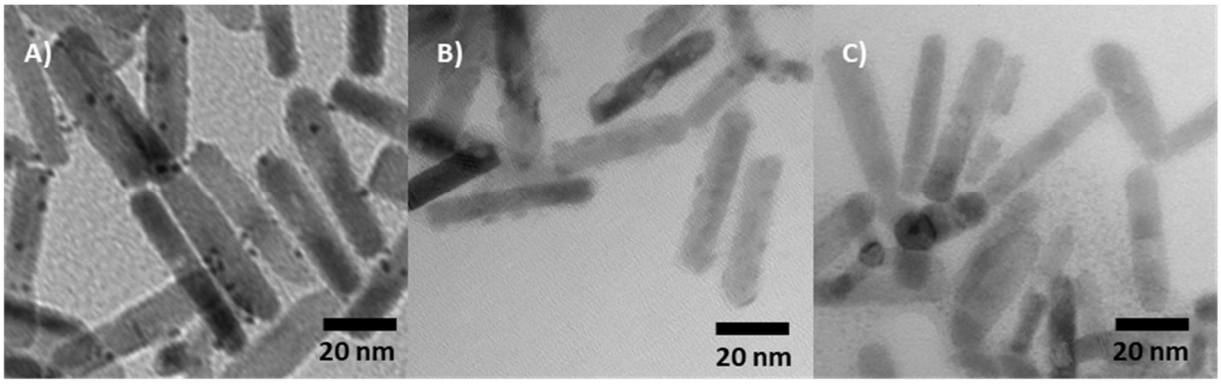

Figure 5.8 TEM images of photodeposition of platinum (Figure 5.8-A), iron (Figure 5.8-B), and nickel (Figure 5.8-C) onto CdSe/CdS nanorods. Platinum deposition onto nanorods was seen clearly from bright field TEM image but iron and nickel decoration could not confirm conclusively.

We were able to get clear HAADF images and EDS maps for platinum decorated CdSe/CdS nanorods but not for iron and nickel decorated nanorods (Figure 5.9). Iron and nickel are in low contrast compared to platinum, maybe due to this we were unable to see the presence of iron and nickel onto our nanorods. We tried to get better images by changing the sample preparation method. The sample was cast onto lacy carbon supported with copper and dried in a vacuum oven at 100°C overnight to get rid of toluene from the sample. We also tried with

different sample holders to get clear images of the samples but still, it was challenging to see metal decoration onto nanorods. We also observed that our nanorods are beam sensitive and degrading for the time being under electron beam exposure.

Figure 5.9 shows the HAADF image and EDS mapping of photo deposited platinum onto CdSe/CdS nanorods. From this HAADF image, bright dots represent platinum deposition onto CdSe/CdS nanorods when the low contrast region is responsible for CdSe/CdS nanorods. EDS mapping image shows Pt decoration (orange colored dot) onto CdSe/CdS nanorods (light blue colored).

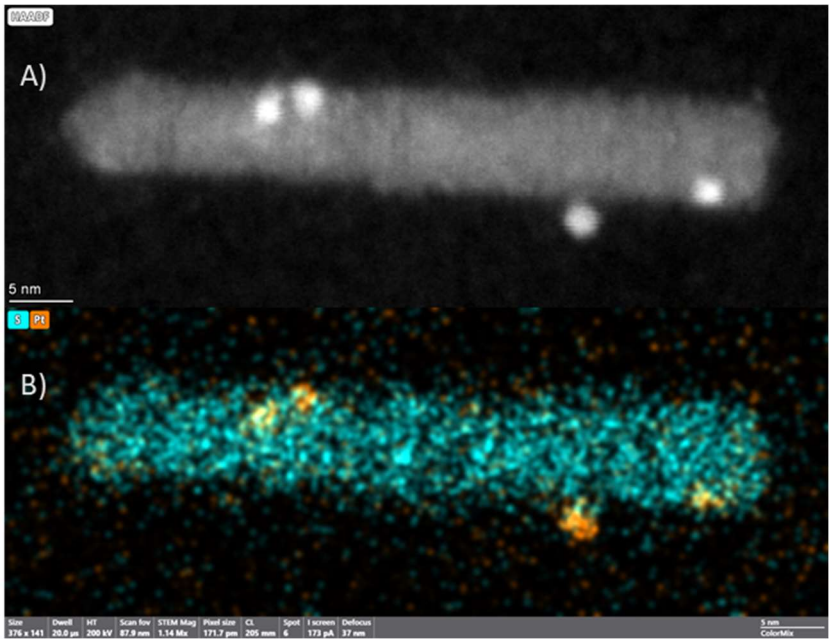

Figure 5.9 A) HAADF image and B)EDS mapping of photo deposited platinum decorated CdSe/CdS nanorods.

5.2.2 Inductively coupled plasma optical emission spectroscopy from photodeposition

Calibration standard solutions containing cadmium, iron, and nickel were prepared by diluting a 1000 ppm standard solution. Five different calibration standards solutions (50 mL) were prepared with nitric acid (10% v/v) as diluting solution (1.0 ppm, 2.5 ppm, 5 ppm, 7.5 ppm, and 10 ppm).

Figure 5.6 shows the standard calibration curve of cadmium, iron, and nickel. This set of calibration standard curves was used to determine the concentration of cadmium, iron, and nickel in the sample. The metal concentration was determined for bare CdSe/CdS nanorods and different photodeposited metals (platinum, iron, and nickel) decorated CdSe/CdS nanorods. Table 5 represents the concentration of metal and the ratio of cadmium to metal in different metal decorated CdSe/CdS nanorods.

Table 5. Cadmium, iron, and nickel concentrations obtained from ICP-OES digestion solutions, and the ratio of cadmium to metal onto metal decorated nanorods synthesis via photodeposition.

Sample	Cd (ppm)	Fe (ppm)	Ni (ppm)	Fe: Cd	Ni: Cd
CdSe/CdS Nanorods	6.38	0.18	0.0	0.03	0
Fe-CdSe/CdS Nanorods	21.32	4.03	0.05	0.19	0
Ni-CdSe/CdS Nanorods	15.41	0.86	7.73	0.06	0.50

5.2.3 Discussion for photodeposition of metals onto CdSe/CdS nanorods

Metal photodeposition onto CdSe/CdS nanorods was achieved by using the illumination of light and a mild reducing agent. Platinum decoration onto nanorods was confirmed from TEM (Figure 5.8-A), HAADF image, and EDS mapping (Figure 5.9) but iron and nickel decoration onto nanorods could not confirm conclusively (Figure 5.8-B and Figure 5.8-C). The concentration of metal present in nanorods and metal decorated nanorods was measured by conducting an ICP-OES analysis. We also observed false signals from ICP-OES for bare CdSe/CdS nanorods and different metal deposited nanorods. The false signals are negligible to metal concentration. Maybe false signals are attributed to the background of the instrument. The ratio of iron to cadmium for iron

decorated CdSe/CdS nanorods is 0.19 while the ratio of nickel to cadmium is 7.73 for nickel decorated nanorods (Table 5). Metal decoration onto nanorods is not confirmed from this ICP-OES data but learned presence and metal concentration onto nanorods.

5.3 Conclusion

The goal of this of this research replace platinum with iron, nickel, or both onto CdSe/CdS nanorods to produce a new photocatalyst. We synthesized CdSe/CdS nanorods by using CdSe quantum dots. CdSe quantum dots and CdSe/CdS nanorods were characterized with optical spectroscopy and electron spectroscopy. Optical spectroscopy and electron microscopy data confirmed the morphology of quantum dots and nanorods. We synthesized two different batches of nanorods from two different batches of CdSe quantum dots because we were trying to deposit metals onto nanorods by using two synthetic routes. One synthetic route was the reduction of metal acetylacetonate salts to metal in the presence of a reducing agent at high temperature and another route was metal photodeposition with the illumination of light in the presence of a mild reducing agent. We used ICP-OES to obtain the relative metal concentrations present in our sample and calculate the ratio of metal to cadmium in different samples, and we used microscopy to get information about metal decoration onto nanorods. TEM was performed for different metal decorated nanorods. Platinum decoration onto CdSe/CdS nanorods was achieved from both synthetic routes. Evidence for the deposition of iron by polyol reduction was also obtained, but EDS mapping after the photodeposition of iron remains to be completed along with EDS mapping after nickel decoration by both polyol reduction and photodeposition.

References

(1) Güney, T. Renewable Energy, Non-Renewable Energy, and Sustainable Development. *International Journal of Sustainable Development & World Ecology* **2019**, *26* (5), 389–397. https://doi.org/10.1080/13504509.2019.1595214.

(2) Dincer, I. Renewable Energy and Sustainable Development: A Crucial Review. *Renewable and Sustainable Energy Reviews* **2000**, *4* (2), 157–175. https://doi.org/10.1016/S1364-0321(99)00011-8.

(3) Gross, R.; Leach, M.; Bauen, A. Progress in Renewable Energy. *Environment International* **2003**, *29* (1), 105–122. https://doi.org/10.1016/S0160-4120(02)00130-7.

(4) Wang, S.; Lu, A.; Zhong, C.-J. Hydrogen Production from Water Electrolysis: Role of Catalysts. *Nano Convergence* **2021**, *8* (1), 4. https://doi.org/10.1186/s40580-021-00254-x.

(5) Yuan, Y.-J.; Chen, D.; Yu, Z.-T.; Zou, Z.-G. Cadmium Sulfide-Based Nanomaterials for Photocatalytic Hydrogen Production. *J. Mater. Chem. A* **2018**, *6* (25), 11606–11630. https://doi.org/10.1039/C8TA00671G.

(6) Gong, M.; Zhou, W.; Tsai, M.-C.; Zhou, J.; Guan, M.; Lin, M.-C.; Zhang, B.; Hu, Y.; Wang, D.-Y.; Yang, J.; Pennycook, S. J.; Hwang, B.-J.; Dai, H. Nanoscale Nickel Oxide/Nickel Heterostructures for Active Hydrogen Evolution Electrocatalysis. *Nat Commun* **2014**, *5* (1), 4695. https://doi.org/10.1038/ncomms5695.

(7) Jakšić, J. M.; Vojnović, M. V.; Krstajić, N. V. Kinetic Analysis of Hydrogen Evolution at Ni–Mo Alloy Electrodes. *Electrochimica Acta* **2000**, *45* (25), 4151–4158. https://doi.org/10.1016/S0013-4686(00)00549-1.

(8) Zhao, Z.; Liu, H.; Gao, W.; Xue, W.; Liu, Z.; Huang, J.; Pan, X.; Huang, Y. Surface-Engineered PtNi-O Nanostructure with Record-High Performance for Electrocatalytic Hydrogen Evolution Reaction. *J. Am. Chem. Soc.* **2018**, *140* (29), 9046–9050. https://doi.org/10.1021/jacs.8b04770.

(9) Suryanto, B. H. R.; Wang, Y.; Hocking, R. K.; Adamson, W.; Zhao, C. Overall Electrochemical Splitting of Water at the Heterogeneous Interface of Nickel and Iron Oxide. *Nat Commun* **2019**, *10* (1), 5599. https://doi.org/10.1038/s41467-019-13415-8.

(10) Kamat, P. V.; Sivula, K. Celebrating 50 Years of Photocatalytic Hydrogen Generation. *ACS Energy Lett.* **2022**, *7* (9), 3149–3150. https://doi.org/10.1021/acsenergylett.2c01889.

(11) Fujishima, A.; Honda, K. Electrochemical Photolysis of Water at a Semiconductor Electrode. *Nature* **1972**, *238* (5358), 37–38. https://doi.org/10.1038/238037a0.

(12) Jafari, T.; Moharreri, E.; Amin, A. S.; Miao, R.; Song, W.; Suib, S. L. Photocatalytic Water Splitting—The Untamed Dream: A Review of Recent Advances. *Molecules* **2016**, *21* (7), 900. https://doi.org/10.3390/molecules21070900.

(13) Highfield, J. Advances and Recent Trends in Heterogeneous Photo(Electro)-Catalysis for Solar Fuels and Chemicals. *Molecules* **2015**, *20* (4), 6739–6793. https://doi.org/10.3390/molecules20046739.

(14) Zhang, L.; Ai, Z.; Xu, X.; Shi, D.; Zhang, B.; Hu, H.; Yang, M.; Shao, Y.; Wu, Y.; Hao, X. Research Progress on Synthetic and Modification Strategies of CdS-Based Photocatalysts. *Ionics* **2023**, *29* (6), 2115–2139. https://doi.org/10.1007/s11581-023-05004-z.

(15) Mohsin, M.; Ishaq, T.; Bhatti, I. A.; Maryam, M.; Jilani, A.; Melaibari, A. A.; Abu-Hamdeh, N. H. Semiconductor Nanomaterial Photocatalysts for Water-Splitting Hydrogen Production: The Holy Grail of Converting Solar Energy to Fuel. *Nanomaterials* **2023**, *13* (3), 546. https://doi.org/10.3390/nano13030546.

(16) Joy, J.; Mathew, J.; George, S. C. Nanomaterials for Photoelectrochemical Water Splitting – Review. International Journal of Hydrogen Energy 2018, 43 (10), 4804–4817. https://doi.org/10.1016/j.ijhydene.2018.01.099.

(17) Lingfeng, Z.; Zhongpan, H.; Xinying, L.; Zhongyong, Y. Noble-Metal-Free Co-Catalysts for TiO2-Based Photocatalytic H2-Evolution Half Reaction in Water Splitting. *Progress in Chemistry* **2016**, *28* (10), 1474. https://doi.org/10.7536/PC160614.

(18) Saraswat, S. K.; Rodene, D. D.; Gupta, R. B. Recent Advancements in Semiconductor Materials for Photoelectrochemical Water Splitting for Hydrogen Production Using Visible Light. *Renewable and Sustainable Energy Reviews* **2018**, *89*, 228–248. https://doi.org/10.1016/j.rser.2018.03.063.

(19) Nasir, J. A.; Rehman, Z. ur; Shah, S. N. A.; Khan, A.; Butler, I. S.; Catlow, C. R. A. Recent Developments and Perspectives in CdS-Based Photocatalysts for Water Splitting. *J. Mater. Chem. A* **2020**, *8* (40), 20752–20780. https://doi.org/10.1039/D0TA05834C.

(20) Tan, W.; Li, Y.; Jiang, W.; Gao, C.; Zhuang, C. CdS Nanospheres Decorated with NiS Quantum Dots as Nobel-Metal-Free Photocatalysts for Efficient Hydrogen Evolution. *ACS Appl. Energy Mater.* **2020**, *3* (8), 8048–8054. https://doi.org/10.1021/acsaem.0c01507.

(21) San Martín, S.; Rivero, M. J.; Ortiz, I. Unravelling the Mechanisms That Drive the Performance of Photocatalytic Hydrogen Production. *Catalysts* **2020**, *10* (8), 901. https://doi.org/10.3390/catal10080901.

(22) Amirav, L.; Alivisatos, A. P. Photocatalytic Hydrogen Production with Tunable Nanorod Heterostructures. *J. Phys. Chem. Lett.* **2010**, *1* (7), 1051–1054. https://doi.org/10.1021/jz100075c.

(23) Carbone, L.; Nobile, C.; De Giorgi, M.; Sala, F. D.; Morello, G.; Pompa, P.; Hytch, M.; Snoeck, E.; Fiore, A.; Franchini, I. R.; Nadasan, M.; Silvestre, A. F.; Chiodo, L.; Kudera, S.; Cingolani, R.; Krahne, R.; Manna, L. Synthesis and Micrometer-Scale Assembly of Colloidal CdSe/CdS Nanorods Prepared by a Seeded Growth Approach. *Nano Lett* **2007**, *7* (10), 2942–2950. https://doi.org/10.1021/nl0717661.

(24) Habas, S. E.; Yang, P.; Mokari, T. Selective Growth of Metal and Binary Metal Tips on CdS Nanorods. *J. Am. Chem. Soc.* **2008**, *130* (11), 3294–3295. https://doi.org/10.1021/ja800104w.

(25) Dukovic, G.; Merkle, M. G.; Nelson, J. H.; Hughes, S. M.; Alivisatos, A. P. Photodeposition of Pt on Colloidal CdS and CdSe/CdS Semiconductor Nanostructures. *Adv. Mater.* **2008**, *20* (22), 4306–4311. https://doi.org/10.1002/adma.200800384.

(26) Ballentine, M. D.; Embry, E. G.; Garcia, M. A.; Hill, L. J. Deposition of Metal Particles onto Semiconductor Nanorods Using an Ionic Liquid. *Beilstein J. Nanotechnol.* **2019**, *10* (1), 718–724. https://doi.org/10.3762/bjnano.10.71.

(27) Schneider, C. A.; Rasband, W. S.; Eliceiri, K. W. NIH Image to ImageJ: 25 Years of Image Analysis. *Nat Methods* **2012**, *9* (7), 671–675. https://doi.org/10.1038/nmeth.2089.

(28) Yu, W. W.; Qu, L.; Guo, W.; Peng, X. Experimental Determination of the Extinction Coefficient of CdTe, CdSe, and CdS Nanocrystals. *Chem. Mater.* **2003**, *15* (14), 2854–2860. https://doi.org/10.1021/cm034081k.

(29) *High-Angle annular dark-field imaging on a tem/stem system - Otten - 1991 - Journal of Electron Microscopy Technique - Wiley Online Library*. https://onlinelibrary.wiley.com/doi/10.1002/jemt.1060170209 (accessed 2023-07-11).

(30) *EDS Analysis | Energy Dispersive Spectroscopy - US*. https://www.thermofisher.com/us/en/home/materials-science/eds-technology.html (accessed 2023-07-11).

(31) Peng, X.; Schlamp, M. C.; Kadavanich, A. V.; Alivisatos, A. P. Epitaxial Growth of Highly Luminescent CdSe/CdS Core/Shell Nanocrystals with Photostability and Electronic Accessibility. *J. Am. Chem. Soc.* **1997**, *119* (30), 7019–7029.

(32) Deka, S.; Falqui, A.; Bertoni, G.; Sangregorio, C.; Poneti, G.; Morello, G.; Giorgi, M. D.; Giannini, C.; Cingolani, R.; Manna, L.; Cozzoli, P. D. Fluorescent Asymmetrically Cobalt-Tipped CdSe@CdS Core@Shell Nanorod Heterostructures Exhibiting Room-Temperature Ferromagnetic Behavior. J. Am. Chem. Soc. 2009, 131 (35), 12817–12828. https://doi.org/10.1021/ja904493c.

Copyright Permission

Name: Nath, Rajib

Email (to receive future readership statistics): rajib.nath898@topper.wku.edu

Type of document: ['Thesis']

Title: TOWARDS DEPOSITION OF IRON AND NICKEL ONTO CADMIUM SELENIDE/CADMIUM SULFIDE NANORODS

Keywords (3-5 keywords not included in the title that uniquely describe content): water splitting, photocatalyst, electrode, semiconductor

Committee Chair: Dr. Lawrence Hill

Additional Committee Members: Dr. Mathew Nee
Dr. Bangbo Yan

Select 3-5 TopSCHOLAR® disciplines for indexing your research topic in TopSCHOLAR®: Chemistry
Physics and Astronomy
School of Engineering and Applied Sciences

Copyright Permission for TopSCHOLAR® (digitalcommons.wku.edu) and ProQuest research repositories:

I hereby warrant that I am the sole copyright owner of the original work.
I also represent that I have obtained permission from third party copyright owners of any material incorporated in part or in whole in the above described material, and I have, as such identified and acknowledged such third-part owned materials clearly. I hereby grant Western Kentucky University the permission to copy, display, perform, distribute for preservation or archiving in any form necessary, this work in TopSCHOLAR® and ProQuest digital repository for worldwide unrestricted access in perpetuity.
I hereby affirm that this submission is in compliance with Western Kentucky University policies and the U.S. copyright laws and that the material does not contain any libelous matter, nor does it violate third-party privacy. I also understand that the University retains the right to remove or deny the right to deposit materials in TopSCHOLAR® and/or ProQuest digital repository.

['I grant permission to post my document in TopSCHOLAR and ProQuest for unrestricted access.']

The person whose information is entered above grants their consent to the collection and use of their information consistent with the Privacy Policy. They acknowledge that the use of this service is subject to the Terms and Conditions.

['I consent to the above statement.']